



**HAL**  
open science

## Fate of Magnetic Nanoparticles during Stimulated Healing of Thermoplastic Elastomers

Angelo Pommella, Pablo Griffiths, Gildas Coativy, Florent Dalmas, Surojit Ranoo, Annette Schmidt, Françoise Méchin, Julien Bernard, Thomas Zinn, Theyencheri Narayanan, et al.

► **To cite this version:**

Angelo Pommella, Pablo Griffiths, Gildas Coativy, Florent Dalmas, Surojit Ranoo, et al.. Fate of Magnetic Nanoparticles during Stimulated Healing of Thermoplastic Elastomers. ACS Nano, 2023, 17 (17), pp.17394-17404. 10.1021/acsnano.3c05440 . hal-04189377

**HAL Id: hal-04189377**

**<https://hal.science/hal-04189377>**

Submitted on 12 Sep 2023

**HAL** is a multi-disciplinary open access archive for the deposit and dissemination of scientific research documents, whether they are published or not. The documents may come from teaching and research institutions in France or abroad, or from public or private research centers.

L'archive ouverte pluridisciplinaire **HAL**, est destinée au dépôt et à la diffusion de documents scientifiques de niveau recherche, publiés ou non, émanant des établissements d'enseignement et de recherche français ou étrangers, des laboratoires publics ou privés.

This document is confidential and is proprietary to the American Chemical Society and its authors. Do not copy or disclose without written permission. If you have received this item in error, notify the sender and delete all copies.

## On the Fate of Magnetic Nanoparticles During Stimulated Healing of Thermoplastic Elastomers

Journal:	ACS Nano
Manuscript ID	nn-2023-054407.R1
Manuscript Type:	Article
Date Submitted by the Author:	28-Jul-2023
Complete List of Authors:	Pommella, Angelo; INSA Lyon, Materials Science Griffiths, Pablo; INSA Lyon, Materials Science Coativy, Gildas; LGEF Dalmas, Florent; Institut National des Sciences Appliquees de Lyon, MATEIS Ranoo, Surojit; Universitat zu Koln, Institut fuer Physikalische Chemie Schmidt, Annette; Universitat zu Koln, Institut fuer Physikalische Chemie MECHIN, Françoise; Institut National des Sciences Appliquees de Lyon, IMP Bernard, Julien; IMP@INSA, IMP/LMM CNRS, UMR5223 Zinn, Thomas; ESRF Narayanan, Theyencheri; ESRF, Experiments Meille, Sylvain; Institut National des Sciences Appliquees de Lyon, MATEIS lab Baeza, Guilhem; INSA Lyon, Materials Science

SCHOLARONE™  
Manuscripts

1  
2  
3  
4  
5  
6  
7  
8  
9  
10  
11  
12  
13  
14  
15  
16  
17  
18  
19  
20  
21  
22  
23  
24  
25

# On the Fate of Magnetic Nanoparticles During Stimulated Healing of Thermoplastic Elastomers

26  
27  
28  
29  
30  
31  
32  
33  
34  
35  
36  
37  
38  
39  
40  
41  
42  
43  
44  
45  
46  
47  
48  
49  
50  
51  
52  
53  
54  
55  
56  
57  
58  
59  
60

Angelo Pommella,<sup>†</sup> Pablo Griffiths,<sup>†,‡</sup> Gildas Coativy,<sup>‡</sup> Florent Dalmas,<sup>†</sup> Surojit  
Ranoo,<sup>¶</sup> Annette M. Schmidt,<sup>¶</sup> Françoise Méchin,<sup>§</sup> Julien Bernard,<sup>§</sup> Thomas  
Zinn,<sup>||</sup> Theyencheri Narayanan,<sup>||</sup> Sylvain Meille,<sup>†</sup> and Guilhem P. Baeza<sup>\*,†</sup>

<sup>†</sup>*Univ Lyon, INSA Lyon, Université Claude Bernard Lyon 1, CNRS, MATEIS, UMR 5510,  
69621 Villeurbanne, France*

<sup>‡</sup>*Univ Lyon, INSA Lyon, Université Claude Bernard Lyon 1, LGEF, EA682, 69621  
Villeurbanne, France*

<sup>¶</sup>*Chemistry Department, Institute for Physical Chemistry, University of Cologne, 50939  
Cologne, Germany*

<sup>§</sup>*Université de Lyon, CNRS, Université Claude Bernard Lyon 1, INSA Lyon, Université  
Jean Monnet, UMR 5223, Ingénierie des Matériaux Polymères F-69621 Villeurbanne  
Cédex, France*

<sup>||</sup>*ESRF, The European Synchrotron, 71 Avenue des Martyrs, CS40220, 38043 Grenoble  
Cedex 9, France*

E-mail: [guilhem.baeza@insa-lyon.fr](mailto:guilhem.baeza@insa-lyon.fr)

## Abstract

We have investigated the heating mechanism in industrially relevant multiblock copolymers filled with Fe-nanoparticles subjected to an oscillatory magnetic field that enables the polymer healing in a contactless manner. While this procedure aims to extend the lifetime of a wide range of thermoplastic polymers, repeated or prolonged stimulus healing is likely to modify their structure, mechanics and ability to heat, which must therefore be characterized in depth. In particular, our work sheds light on the physical origin of the secondary heating mechanism detected in soft systems subjected to magnetic hyperthermia, being triggered by the copolymer chains dissociation. In spite of earlier observations, the origin of this additional heating remained unclear. By using both static and dynamic X-ray scattering methods (small angle X-ray scattering and X-ray photon correlation spectroscopy, respectively), we demonstrate that beyond magnetic hysteresis losses, the enormous drop of viscosity at the polymer melting temperature enables motion of nanoparticles that generates additional heat through friction. Besides, we show that applying induction heating for a few minutes is found to magnetize the nanoparticles, which causes their alignment into dipolar chains and leads to non-monotonic translational dynamics. By extrapolating these observations to rotational dynamics and the corresponding amount of heat generated through friction, we not only clarify the origin of the secondary heating mechanism but we also rationalize the presence of possible temperature maxima observed during induction heating.

## Keywords

thermoplastic elastomers, multiblock copolymers, magnetic nanoparticles, induction heating, stimulus-healing, nanocomposite, XPCS, SAXS

1  
2  
3 Thermoplastic elastomers (TPE) made of  $(AB)_n-A$  multiblock copolymers have emerged  
4 in the mid twentieth century and are under constant development since then.<sup>1-3</sup> Their great-  
5 est asset with respect to vulcanized rubbers resides in their ability to switch between the  
6 solid- and the liquid-state upon temperature change, which enables their easy processing  
7 through conventional extrusion and injection as well as more recent additive manufacturing  
8 methods. While they (almost) behave as homogeneous polymer melts at temperatures above  
9 the dissociation point of their hard-segments ( $B=HS$ ), they possess elastomer-like properties  
10 at room temperature owing to the presence of amorphous and/or crystalline HS assemblies  
11 encompassed in low-glass transition temperature ( $T_g$ ) soft-segments ( $A=SS$ ). Beyond pro-  
12 cessing aspects, their thermo-reversibility also appears as a unique opportunity to repair,  
13 reshape and reuse them.  
14  
15  
16  
17  
18  
19  
20  
21  
22  
23  
24

25 Unlike self-healing in soft materials,<sup>4</sup> the healing of strong TPEs is based on their solid-  
26 to-liquid phase transition and requires therefore the application of a stimulus that can take  
27 various physical forms, among which convective heat, mechanical friction, microwaves, sol-  
28 vent impregnation or magnetic field. In the latter case, TPEs are filled with magnetic parti-  
29 cles capable to convert the applied oscillatory magnetic excitation into heat through different  
30 mechanisms according to their size and nature.<sup>5</sup> While electrically conductive particles larger  
31 than a few millimeters can generate *eddy* currents that heat the materials through Joule ef-  
32 fect, nano- and micro-particles produce heat through Weiss domains walls motion regardless  
33 of their electric conductivity. Even smaller superparamagnetic nanoparticles (NPs) can dis-  
34 sipate heat through Néel and Brownian relaxations.<sup>6</sup> The main asset of induction healing  
35 resides in its flexibility since the heat generated within the composite not only depends on  
36 the particles' nature, size, shape and volume fraction ( $\phi$ ) but also on the characteristics of  
37 the magnetic field such as its frequency ( $f$ ) and its amplitude ( $H$ ). To a lesser extent, the  
38 magnetic history (i.e., the configuration of macro-spins) and the particles dispersion (im-  
39 pacting dipolar interactions) also modify the particles ability to heat. The latter parameter  
40 is commonly named "specific absorption rate" (SAR)<sup>6</sup> and is approximately  $65 Wg^{-1}$  in  
41  
42  
43  
44  
45  
46  
47  
48  
49  
50  
51  
52  
53  
54  
55  
56  
57  
58  
59  
60

1  
2  
3 the present work. Besides, induction heating is a contactless method allowing to apply the  
4 stimulus through thin materials layers, being notably relevant for adhesives applications.<sup>7</sup>  
5  
6 The limited penetration depth owing to the decrease of the magnetic field amplitude with  
7 the coil-sample distance also enables to realize surface treatment without altering the bulk  
8 structure of homogeneous composites.<sup>8</sup> Alternatively, the localization of responsive fillers  
9 in a macro-architected material can be used to melt selectively certain parts of it. This  
10 versatility and the growing need for lifetime extension of thermoplastics-based engineering  
11 goods make materials-healing oriented "magnetic hyperthermia" a promising technique to  
12 support sustainable development.  
13  
14  
15  
16  
17  
18  
19  
20

21 Although induction heating is used for more than a century in various applications,  
22 its utilization for materials healing is more recent and has strongly grown in the last two  
23 decades, contemporaneously with major progresses in chemistry. In 2009, the pioneering  
24 work of Corten and Urban notably showed the possibility to repair a fluorinated terpolymer  
25 filled with  $\gamma$ -Fe<sub>2</sub>O<sub>3</sub> NPs by means of magnetic hyperthermia.<sup>9</sup> The group of Ramanujan  
26 also developed promising healable rubbers based on copolymers either poly(ethylene-vinyl  
27 acetate) (PEVA)<sup>10</sup> or acrylonitrile butadiene (NBR).<sup>11</sup> The same philosophy was used by the  
28 group of Schmidt with ionomers, where the elasticity of the rubber relied on the aggregation  
29 of ionic groups rather than the polymer crystallization.<sup>12</sup> Remarkably, the optimization of the  
30 material's formulation and stimulus by Yang et al. further allowed to formulate repairable  
31 homopolymers with an extremely low fraction of responsive fillers ( $< 0.25$  vol.%) capable of  
32 migrating selectively towards microcracks before healing and subsequent rehomogenization.<sup>13</sup>  
33  
34  
35  
36  
37  
38  
39  
40  
41  
42  
43  
44

45 Recently, we have performed a multi-physics characterization of a thermoplastic polyurethane  
46 (TPU) filled with either Fe or Fe<sub>3</sub>O<sub>4</sub> particles with the aim to identify a list of criteria en-  
47 abling to improve the design of healable rubbers.<sup>8,14</sup> Of particular interest, magnetic particles  
48 were seen to trigger an extra heating source from the melting of the TPU in addition to the  
49 expected heating mechanisms activated right from the application of the oscillatory stim-  
50 ulus. This phenomenon was also detected in metal-ligand based supramolecular networks  
51  
52  
53  
54  
55  
56  
57  
58  
59  
60

1  
2  
3 filled with identical Fe NPs, confirming that beyond the chemical nature of the polymer  
4 host, the sudden fall of viscosity caused by the deactivation of topological links was respon-  
5 sible for the extra-heating.<sup>15</sup> Similar results were obtained by Hiergeist et al. in relatively  
6 dense gels filled with 100 nm NPs where the extra-heating appeared around 30 °C<sup>16</sup> and  
7 by Bayerl et al. in semi-crystalline homopolymers filled with micronic particles where the  
8 extra-heating was particularly visible from ca. 130 °C.<sup>17</sup> In these articles, the extra-heating  
9 was rationalized by invoking mechanical friction occurring between the magnetic particles  
10 and their viscous surroundings, the corresponding motion being only possible at low enough  
11 viscosity. In our case, the presence of dipolar chains after the application of the healing  
12 procedure<sup>8</sup> well supported the hypothesis of NPs translational motion over several hundreds  
13 of nanometers, likely to be accompanied with rotational friction as modeled by Yassine et  
14 al.<sup>18</sup> and Helbig et al.<sup>19</sup> Nevertheless, a direct *in situ* experimental evidence confirming this  
15 scenario was still lacking.

16  
17  
18  
19  
20  
21  
22  
23  
24  
25  
26  
27  
28  
29 In this work, we use *in situ* time-resolved ultra small-angle X-ray scattering (USAXS)  
30 and X-ray photon correlation spectroscopy (XPCS) to investigate the microscopic structure  
31 and the collective microscopic dynamics during induction heating of a nanocomposite made  
32 of thermoplastic polyurethane filled with 5 *vol.*% of iron NPs (denoted 5% Fe-n hereafter)  
33 already introduced in our previous paper.<sup>8</sup> We start by investigating the sample structure  
34 at room temperature and then follow the evolution of its temperature and microstructure  
35 during the application of an oscillatory magnetic field. We subsequently study the collective  
36 microscopic dynamics of the sample at high temperature both in absence (hot stage) and  
37 in presence (double turn coil) of the magnetic stimulus to elucidate the evolution of the  
38 dynamical behavior of NPs during the healing procedure.  
39  
40  
41  
42  
43  
44  
45  
46  
47  
48  
49  
50  
51  
52  
53  
54  
55  
56  
57  
58  
59  
60

# Results and discussion

## Nanocomposite microscopic structure

### Microstructure in zero field

Figure 1a shows the measured (U)SAXS intensity profiles at 25 °C for the TPU matrix, the 5% Fe-n composite and the Fe-n powder covering a  $q$ -range from  $q = 2 \times 10^{-3}$  to  $2 \text{ nm}^{-1}$  (or  $5 \text{ nm}^{-1}$  for the powder). The polymer matrix shows an expected correlation peak at  $q_{TPU}^* \approx 0.4 \text{ nm}^{-1}$  corresponding to the most probable distance between ribbon-like crystallites,<sup>8</sup>  $\xi_{TPU} = \frac{2\pi}{q_{TPU}^*} \approx 15 \text{ nm}$ . The  $q^{-4}$  low- $q$  upturn is most likely caused by micron-scale voids as already observed in other multiblock copolymers<sup>20</sup> and is thus not representing any particular structural feature. On the other hand, (U)SAXS performed on the Fe-n powder reveals a multiscale organization. First, a narrow Porod regime characterized by  $I \sim q^{-4}$  is observed at  $q > 2 \text{ nm}^{-1}$  indicating that the surface of Fe-n NPs is smooth. A first break in slope is then observed at  $q_{1-Fe} = 1.1 \text{ nm}^{-1}$ , most likely emerging from the presence of a thin layer of iron-oxide (ca.  $3 \text{ nm}$ ) at the NPs surface.<sup>21</sup> At  $q < q_{1-Fe}$ , the scattering intensity keeps on increasing like  $q^{-4}$  before exhibiting a shoulder close to  $q_{2-Fe} = 7 \times 10^{-2} \text{ nm}^{-1}$  corresponding to the mean diameter of NPs close to  $84 \text{ nm}$ . While the same observation is expectedly made on the composite, it shows, at lower  $q$ , a fractal regime characterized by  $I \sim q^{-2.7}$  before reaching a quasi-plateau whereas the signal diverges for the powder. In the former case, the scattering intensity emphasizes the aggregation of NPs into finite size objects close to the micron lengthscale as confirmed by TEM observations reported in Figure 1b and in our previous work.<sup>8</sup> In the latter case, the divergence is caused by refraction and multiple scattering owing to the much higher volume fraction of scatterers in the powder. The magnetic characterization of the non-irradiated composite and the powder are provided in the first part of the Supporting Information section 1.

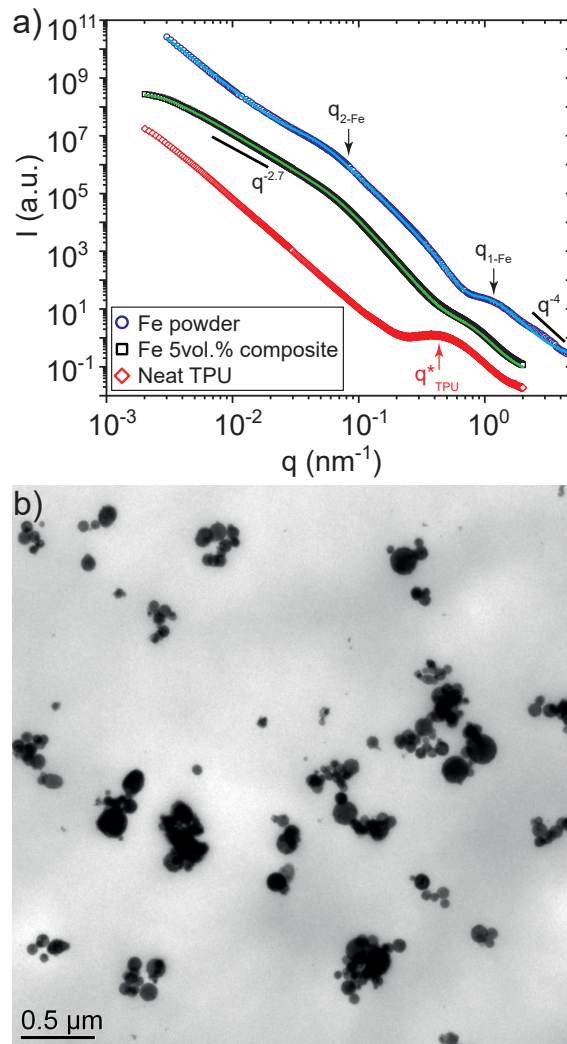


Figure 1: a) (U)SAXS intensity at 25 °C of the Neat TPU (red diamonds), the 5% Fe-n composite (black squares) and the corresponding Fe-n powder (blue circles). Data are shifted vertically for clarity. Solid lines are fit to the powder and composite data with the unified scattering function<sup>22</sup> providing a NP diameter of  $84 \pm 1 \text{ nm}$ .  $q_{TPU}^*$ ,  $q_{1-Fe}$  and  $q_{2-Fe}$  are respectively correlated with the TPU inter-crystallites distance, the NP surface state (iron-oxide layer) and the NPs mean size. b) TEM micrograph of the corresponding 5% Fe-n composite.

## Structural and thermal evolution under magnetic field

In order to probe possible NPs aggregates motion occurring during the healing procedure, we investigated the structural evolution of the NPs in a 5% Fe-n composite during induction heating by means of time-resolved USAXS. 2D scattering patterns were acquired every 1 second (exposure time  $\approx 100$  ms) starting from the activation of the magnetic field and for a total duration of 20 min. The sample microstructure was observed in the  $q$ -range  $2 \times 10^{-3} - 6 \times 10^{-2} \text{ nm}^{-1}$  to focus on lengthscales corresponding approximately to the size of the NP aggregates. A first qualitative observation of the 2D scattering patterns (reported in Supporting Information section 2) emphasizes the impact of the oscillatory magnetic field on the NPs structure. Indeed, while the USAXS pattern is fully isotropic at the beginning of the experiment, it has clearly become anisotropic after 20 min of irradiation. More quantitatively, we report both horizontal and vertical integration of the 2D patterns in Figures 2a and 2b, respectively for  $t < 0$  and  $t = 20$  min. The scattering intensity measured before the activation of the magnetic field shows the same intensity power-law decay ( $I \sim q^{-n}$ ) along the horizontal and vertical directions with an exponent ( $n = \frac{d \log I(q)}{d \log q}$ ) corresponding to 2.7 in the  $q$ -range  $9 \times 10^{-3} - 6 \times 10^{-2} \text{ nm}^{-1}$ , identically as in the previous section. In contrast, the intensity decay becomes anisotropic at the end of the experiment with an exponent  $n = 3$  for the horizontal direction and  $n = 2.4$  for the vertical one. This result indicates a preferential alignment of NP aggregates in the vertical direction that is parallel to the magnetic field lines. The intensity is lower in the vertical direction because of the growing influence of the structure factor "correlation hole"<sup>23</sup> at  $q < q_{2-Fe}$  resulting from the oriented chain-like aggregates formation. Besides, the leveling-off of the power-law found at  $q < 9 \times 10^{-3} \text{ nm}^{-1}$  in Figure 1a is no longer present here. This is explained by the appearance of very large NP agglomerates with size bigger than  $1 \mu\text{m}$  allowed by NPs translational motion and favorable dipolar interactions. FIB-SEM micrographs inserted in Figure 2a and 2b taken respectively before and after the induction heating confirm this interpretation, emphasizing the emergence of vertical dipolar chains.

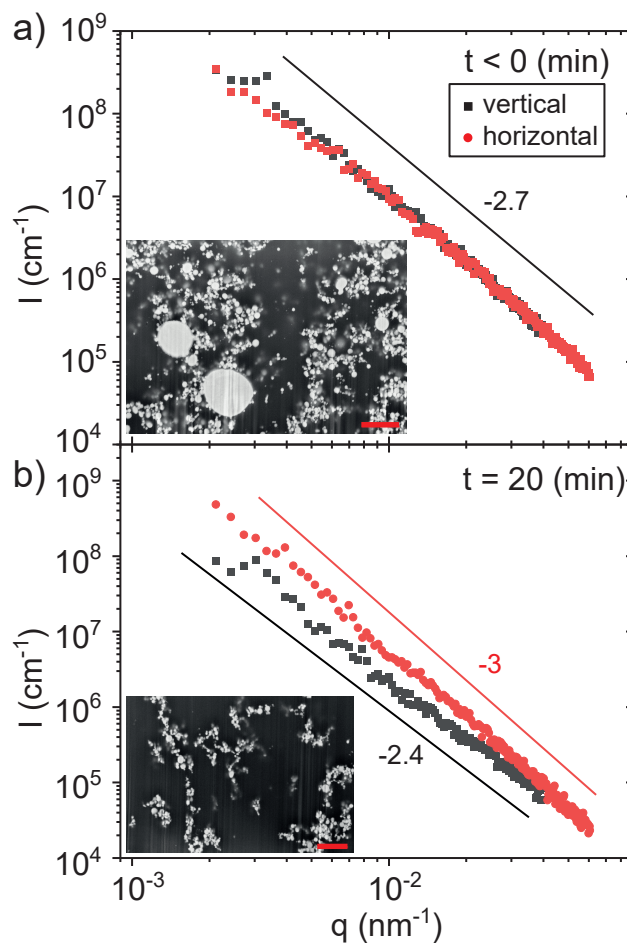


Figure 2: USAXS intensity as a function of the scattering vector of the 5% Fe-n composite before (a) and at the end (b) of the induction heating. The solid lines are guides for the eye. Insets: FIB-SEM cross-section micrographs of the same material before (a) and after (b) the induction heating applied in the configuration reported in ref. 8. Large visible spheres in (a) belong to the broad particle size distribution. These images were taken at room temperature. The red dimensional bars are  $1 \mu\text{m}$ .

The above-mentioned structural changes must be put in parallel with the evolution of the material's temperature during the procedure. As shown in Figure 3a, the activation of the oscillatory magnetic field at time  $t = 0$  induces an immediate rise of the sample temperature  $T$  that passes through a maximum  $T_{\max} = 210 \pm 1 \text{ }^\circ\text{C}$  at  $t_{T_{\max}} \approx 3.3 \text{ min}$  before stabilizing at  $T_{\text{plateau}} = 187 \pm 1 \text{ }^\circ\text{C}$  after 15 *min*. For the sake of data storage, the temperature was measured in a continuous way during the first 15 *min* (see materials and methods) and then measured punctually at the end of the experiment to verify its stability. Importantly, the highest measured temperature  $T_{\max}$  remained well-below the commonly accepted degradation point of alkyl-urethane-alkyl groups present in our TPU close to  $250 \text{ }^\circ\text{C}$ .<sup>24</sup> In the Figure 3a inset, we magnified the data of the first 3.5 *min* evidencing that as long as the sample remains in the solid state ( $T < 100 \text{ }^\circ\text{C}$ ), the temperature rises according to

$$T = T_0 + \Delta T \left[ 1 - \exp\left(-\frac{t}{\tau_T}\right) \right]. \quad (1)$$

This expression is the 0-dimension solution of the heat equation for a constant energy flux (also referred as the Box-Lucas equation) where  $T_0$ ,  $\Delta T$  and  $\tau_T$  are respectively the room temperature, the amplitude of the temperature rise and the characteristic time of the exponential function.<sup>25,26</sup> This simple thermal evolution is expected when a constant incident power is compensated by heat loss (mainly convection here). At short time ( $t < 15 \text{ s}$ ), Eq.1 can be used to fit satisfyingly the data with  $T_0 = 21.7 \text{ }^\circ\text{C}$ ,  $\Delta T = 106.54 \text{ }^\circ\text{C}$  and  $\tau_T = 8.91 \text{ s}$ , indicating that a single heating mechanism is involved, which consists of magnetic hysteresis losses caused by Weiss domain wall motion occurring in our multidomain NPs.<sup>8</sup> Extrapolating the fit up to 3.5 *min* however emphasizes a strong mismatch with the data (see the red line in Figure 3a inset). While one would have expected the temperature to saturate in the case of a constant energy flux, the temperature is conversely observed to increase continuously above the TPU melting point (spanning from 100 to  $150 \text{ }^\circ\text{C}$  in DSC<sup>8</sup>) until reaching a maximum ca. 3 *min* later. As already proposed in the literature,<sup>8,15-17</sup> we assign this

1  
2  
3 extra-heating to the friction of NPs with their viscous environment, suddenly made possible  
4 by the gigantic drop of viscosity occurring at the TPU melting point. Note that alternative  
5 explanations involving a strong evolution of the heat capacity of the composite or impor-  
6 tant changes of magnetic properties likely to increase the hysteresis loop are not satisfying.  
7 In fact, the heat capacity of our polymer remains almost unchanged in this temperature  
8 range because it is far above the glass transition temperature of the polymer and that its  
9 crystallinity is quite weak (10 wt.%). On the other hand, the magnetic properties of irradi-  
10 ated samples were measured both in the parallel and perpendicular directions with respect  
11 to the magnetic field used for induction heating, showing no significant evolution with re-  
12 spect to the non-irradiated sample (see the second part of Supporting Information section 1).  
13  
14  
15  
16  
17  
18  
19  
20  
21  
22  
23  
24

25 Two important insights in the evolution of the microscopic structure with time are re-  
26 ported in Figure 3b, where the temporal variations of the "horizontal" and "vertical" power-  
27 law exponents  $n$  are shown over the entire induction heating experiment. This figure first  
28 reveals that after a brief period of stability of ca. 30 s, the exponents diverge progressively  
29 before stabilizing after almost 3.3 min. This structural evolution must be correlated with the  
30 thermal one reported in Figure 3a where the extra-heating was also observed to start after ca.  
31 30 s, showing subsequently a maximum in temperature around 3.3 min. Coupling structural  
32 and thermal information therefore strongly supports the hypothesis that NP aggregates mo-  
33 tion (and corresponding friction) is at the very origin of the extra-heating process. Secondly,  
34 the fact that the power-law exponents reach their final plateau after ca. 3.3 min indicates  
35 that the static (time averaged) structure of the NPs does not evolve anymore from this stage.  
36 Interestingly, because this time matches the position of  $T_{\max}$  reported in Figure 3a, these  
37 observations suggest a progressive diminution of the extra-heating process amplitude with  
38 time once the structural equilibrium is reached. In other words, they suggest that while it  
39 is suddenly promoted by the polymer melting at the beginning of the experiment, the NPs  
40 motion becomes hindered at long time because of the formation of dipolar chains.  
41  
42  
43  
44  
45  
46  
47  
48  
49  
50  
51  
52  
53  
54  
55  
56  
57  
58  
59  
60

1  
2  
3 The important message emerging from this first part is that we now have strong exper-  
4 imental evidences that NP aggregates motion is the microscopic mechanism controlling the  
5 extra-heating process observed during induction heating and is therefore likely to impact  
6 the properties of the after healing materials. We however still lack information concerning  
7 the dynamical character of the motion, notably to rationalize the presence of a maximum  
8 in the temperature evolution. To progress in this direction, we present in the next section a  
9 systematic XPCS characterization performed under the same conditions.  
10  
11  
12  
13  
14  
15  
16  
17  
18  
19  
20  
21  
22  
23  
24  
25  
26  
27  
28  
29  
30  
31  
32  
33  
34  
35  
36  
37  
38  
39  
40  
41  
42  
43  
44  
45  
46  
47  
48  
49  
50  
51  
52  
53  
54  
55  
56  
57  
58  
59  
60

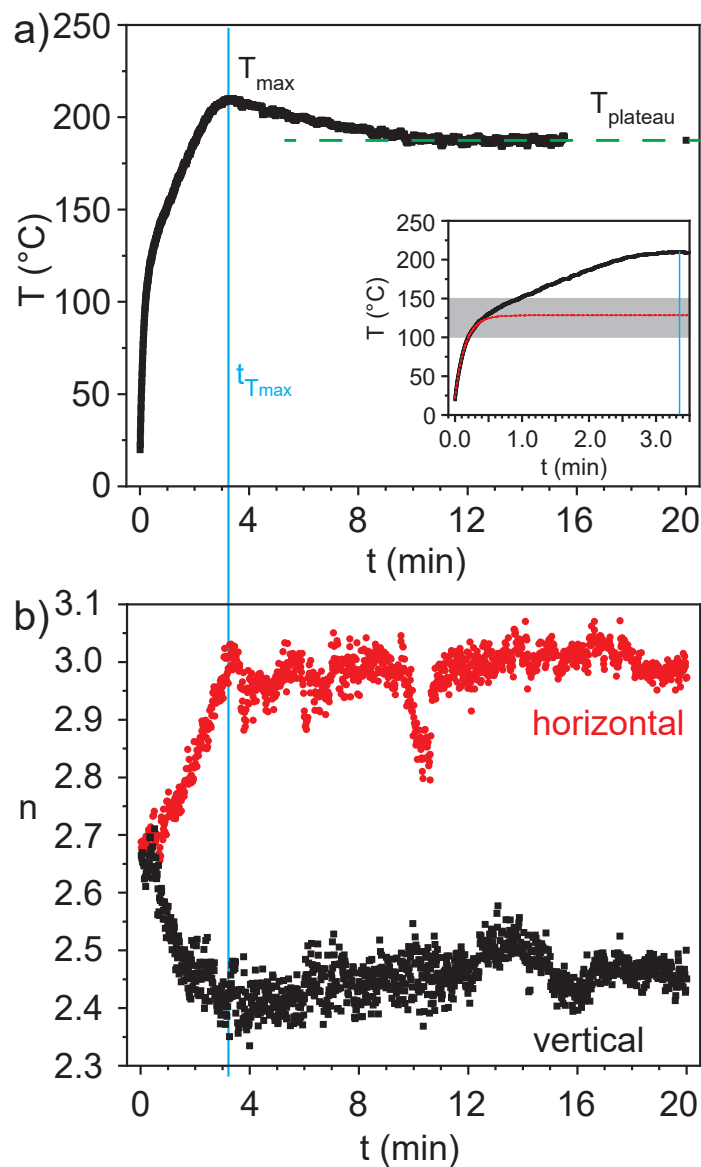


Figure 3: a) Temperature variation of the 5% Fe-n composite upon induction heating measured by an infrared-camera over the entire experimental time (20 min). The final plateau value of the temperature ( $T_{\text{plateau}}$ ) is  $187 \pm 1$  °C. The inset is a zoom-in representation showing the temperature rise during the first 3.5 min. The red line is obtained by fitting the experimental data from  $t = 0$  to  $t = 15$  s according to Eq. 1. The grey area indicates the region where the melting of the polymer matrix (TPU) takes place. b) Temporal variation of the horizontal and vertical power-law exponents  $n$  over the entire induction heating experiment. The  $q$ -range is  $9 \times 10^{-3} - 6 \times 10^{-2} \text{ nm}^{-1}$ . The vertical blue solid line indicates the time at which  $T_{\text{max}}$  is observed.

## Nanocomposite collective microscopic dynamics

In this section, we investigate the collective microscopic dynamics of the 5% Fe-n composite to study the displacement of NPs aggregates within the TPU matrix. We decouple the thermal and magnetic contributions to the collective dynamics at ca.  $T = 180\text{ }^{\circ}\text{C}$  by using either a hot-stage or our purpose-made magnetic induction setup to heat the samples.

### Collective dynamics in absence of magnetic field

The collective microscopic dynamics of the 5% Fe-n composite in absence of magnetic field was characterized through *in situ* X-ray photon correlation spectroscopy (XPCS) to measure the local motion of NPs aggregates. After reaching the desired temperature of  $180\text{ }^{\circ}\text{C}$ , we waited for 5 *min* for thermal equilibrium before starting the data acquisition. The temporal fluctuations of the pixel intensities were quantified in terms of the intensity-intensity autocorrelation function  $g_2(\mathbf{q}, \tau)$  (see eq. 5 in the materials and methods section) that provides information on the microscopic dynamics through the intermediate scattering function  $f(\mathbf{q}, \tau)$  obtained by the Siegert relation  $g_2(\mathbf{q}, \tau) = 1 + B(f(\mathbf{q}, \tau))^2$  with  $B$  the speckle contrast such that  $f(\tau \rightarrow 0) = 1$ . The intermediate scattering function represents the normalized autocorrelation function of density fluctuations of NPs aggregates and it quantifies their collective microscopic dynamics projected onto the scattering vector. It can be empirically described by using the Kohlrausch-Williams-Watts (KWW) function:

$$f(\mathbf{q}, \tau) = \exp \left[ - \left( \frac{\tau}{\tau_0(\mathbf{q})} \right)^{\beta(\mathbf{q})} \right] \quad (2)$$

where  $\tau_0$  is the relaxation time and  $\beta$  is the KWW exponent that depends on the sample dynamics. By replacing Eq. 2 in the Siegert relation, one then obtains the following expression describing the decay of the normalized  $g_2(\mathbf{q}, \tau)$  function

$$\frac{g_2(\mathbf{q}, \tau) - 1}{B} = \exp \left[ -2 \left( \frac{\tau}{\tau_0(\mathbf{q})} \right)^{\beta(\mathbf{q})} \right]. \quad (3)$$

1  
2  
3 that is used to fit the data in Figure 4. Note that because of the strong dependence of  $\tau_0$   
4 with the exponent  $\beta$ , it is convenient to calculate an average characteristic relaxation time  
5  $\tau_c = \tau_0/\beta \Gamma(1/\beta)$  where  $\Gamma(\cdot)$  denotes the Gamma function.<sup>27</sup>  
6  
7

8  
9 The autocorrelation functions presented below were systematically obtained by analyzing  
10 the scattering intensity variations along the sole horizontal direction of the speckle images  
11 as indicated by the red dashed line in Figure S2 (Supporting Information section 2). This  
12 choice ruled out any contribution from the collective microscopic dynamics coming from  
13 the affine motion caused by the vertical gravity-driven flow of the sample. For the sake of  
14 completeness, we nevertheless report in Supporting Information section 3 the analysis of the  
15 dynamics along the vertical direction.  
16  
17  
18  
19  
20  
21  
22

23 We present in Figure 4 the normalized autocorrelation functions obtained at 180 °C  
24 in absence of magnetic field for different scattering vector moduli (open symbols) as well  
25 as the one obtained at 35 °C and  $q = 0.058 \text{ nm}^{-1}$  (closed symbols). The variation of  $q$   
26 allows us to probe the relaxation time on length scales  $\sim 2\pi/q$  ranging from  $\approx 100 \text{ nm}$  to  
27  $\approx 2 \mu\text{m}$ , corresponding to displacements comparable to the aggregate size. Here, it clearly  
28 appears that when  $T = 180 \text{ °C}$  all autocorrelation functions decorrelate completely over the  
29 investigated timescale whereas the one at  $T = 35 \text{ °C}$  does not show any decorrelation in the  
30 same time-window. This striking difference is explained by the fact that the polymer matrix  
31 is liquid-like at 180 °C enabling NPs motion, whereas it is solid-like at 35 °C, drastically  
32 slowing down the collective dynamics of NPs.  
33  
34  
35  
36  
37  
38  
39  
40  
41  
42

43 Remarkably, the autocorrelation functions obtained at 180 °C were found to decorrelate  
44 as compressed exponential functions ( $\beta > 1$  in Eqs. 2-3) as shown in the inset of Figure 4  
45 where  $\tau_c$  and  $\beta$  were obtained by fitting the experimental data with Eq. 3.  $\beta$  values were  
46 found to be constant and close to  $1.58 \pm 0.04$  indicating that our sample is characterized  
47 by hyperdiffusive dynamics, being similar to the compressed exponential relaxation of inter-  
48 nal stress reported for different out-of-equilibrium systems such as gels,<sup>28,29</sup> suspensions<sup>30</sup>  
49 and polymer-based materials.<sup>31,32</sup> Because of the biphasic nature of the host TPU and the  
50  
51  
52  
53  
54  
55  
56  
57  
58  
59  
60

gravity-driven flow, our sample is actually out of equilibrium, which necessarily induces local rearrangements of NPs aggregates with a consequent build-up of internal stress that, unlike in Brownian fluids, does not relax instantaneously but rather propagates in the surrounding matrix. Moreover, preferential interactions of the NPs with the polar blocks of the TPU (already evidenced by DSC in ref. 8), are also very likely to contribute to the formation of internal stress. Indeed, preferential interactions induce a continuous evolution of the strain field when changing the temperature, being possibly responsible of the compressed exponential profile as already found in nanocomposites.<sup>32</sup>

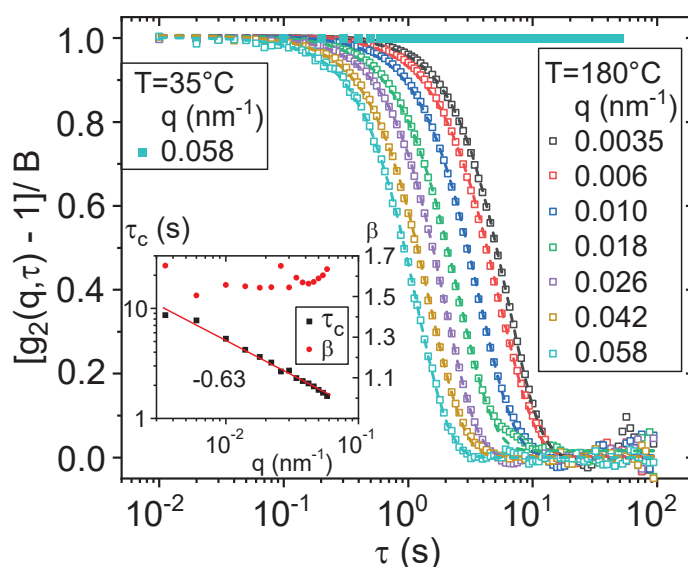


Figure 4: Normalized intensity-intensity autocorrelation functions at different scattering vector moduli for the 5% Fe-n composite at 35 °C (closed symbols) and 180 °C (open symbols) in the absence of magnetic field. Dashed lines are fit to the experimental data according to Eq. 3. Inset: characteristic decorrelation time ( $\tau_c$ ) and exponent ( $\beta$ ) obtained from the fit of the intensity-intensity autocorrelation functions at 180 °C shown in the main figure. The solid line is a power-law fit of  $\tau_c(q)$  providing an exponent of  $-0.63 \pm 0.02$ .

In Figure 4 inset, the time  $\tau_c$  is seen to decrease with the scattering vector modulus following a power-law dependence characterized by an exponent  $-0.63 \pm 0.02$ . Interestingly, a similar value of  $-0.5$  was observed in the collective dynamics of magnetic particles embedded in a natural rubber matrix in presence of a magnetic stimulus.<sup>33</sup> However, the authors did

not investigate specifically the origin of this scaling that was assigned to a possible crossover between different dynamical regimes. In our case, these dynamical regimes could originate from the large size polydispersity of the NPs aggregates as well as from the complex nature of the host polymer and its interaction with the NPs. While in hyperdiffusive dynamics, the average characteristic time  $\tau_c$  is usually expected to vary with  $q^{-1}$ , which allows to define a ballistic velocity  $v = \frac{1}{\tau_c q}$  across several lengthscales, this dependence was observed and theoretically predicted for homogeneous host fluids only such as Newtonian solvents or homopolymer melts.<sup>28,29,32</sup> This assumption is obviously no longer valid for our block copolymer matrix, including above its melting point where a certain degree of phase separation is known to persist. This remaining structuration in the liquid state is notably detectable through frequency sweep rheological tests revealing the presence of a low-frequency storage modulus plateau above the melting point<sup>3,34,35</sup> as it is the case for the present TPU matrix ( $G'_{\omega \rightarrow 0} \approx 30 \text{ Pa}$  in ref. 8). Based on the rubber elasticity theory, we estimate the distance between hard-segments rich domains to ca.  $60 \text{ nm}$  at  $180 \text{ }^\circ\text{C}$ , that is, in average, ten times smaller than the size (from  $0.2 \text{ }\mu\text{m}$  to  $1 \text{ }\mu\text{m}$ ) of the NP aggregates (see Supporting Information section 4).

To summarize, the unexpected hyperdiffusive dynamics ( $\tau_c \sim q^{-0.63}$ ) observed in absence of magnetic field might be rationalized by invoking different arguments that could be tested in the future with model samples:

- The collective dynamics observed is a superposition of non-affine and affine contributions, in particular larger scale advection of NPs and their clusters, which can lead to an effective weaker  $q$ -dependence.<sup>36</sup>
- The large polydispersity of the NPs and corresponding aggregates is likely to generate qualitatively different dynamical behaviors.
- Favorable enthalpic interactions existing between the NPs surface and the polar blocks of the TPU is very likely to impact the NPs dynamics according to their size through

1  
2  
3 the number of physical bonds existing between each NP (or aggregate) and the host  
4 polymer. These interactions were evidenced by DSC in our previous work.<sup>8</sup>  
5  
6

- 7
- 8 • The soft mesh formed by the remaining phase separation of the TPU in the liquid  
9 state is expected to perturb the NPs motion since its average cell-parameter (60 nm)  
10 is smaller than the NPs mean diameter.  
11  
12  
13

### 14 15 16 17 18 **Collective dynamics under oscillatory magnetic field**

19  
20 In the following, we present the collective microscopic dynamics of the 5% Fe-n composite  
21 in presence of an oscillatory magnetic field. During induction heating, we performed two  
22 XPCS data acquisitions to investigate the collective dynamics both at early stage, when  
23 the sample microstructure is evolving rapidly ( $t < t_{T_{\max}}$ ), and after a reasonably long time,  
24 when the microstructure has reached a stable configuration ( $t > t_{T_{\max}}$ ). To compare these  
25 experimental data to the ones obtained without magnetic field reported in the previous  
26 section, we started the two acquisitions when the temperature was as close as possible to  
27 180 °C corresponding to  $t = 2 \text{ min}$  and  $t = 19 \text{ min}$  of induction heating (Figure 3b). At  
28  $t = 2 \text{ min}$ , the acquisition lasted 10 s during which the sample temperature varied from 186  
29 °C to 190 °C (see Figure 5). For this reason, we considered that the collective dynamics was  
30 investigated at an average temperature of  $188 \pm 2 \text{ °C}$ . At  $t = 19 \text{ min}$ , the temperature was  
31 considered constant at  $187 \pm 1 \text{ °C}$  (see Figure 6). Despite the fact that the temperature is  
32 in both cases slightly above the one set by our hot-stage in the previous section (180 °C),  
33 we believe that it is close enough to allow a good comparison of the data, making it possible  
34 to isolate the impact of the magnetic contribution on the NPs dynamics.  
35  
36  
37  
38  
39  
40  
41  
42  
43  
44  
45  
46  
47  
48  
49

50 In Figure 5, we present the normalized autocorrelation functions obtained at  $t = 2 \text{ min}$ .  
51 As compared to the previous case without magnetic field, they exhibit here a bimodal pro-  
52 file, which overall decorrelates ten times faster. We attribute the corresponding "fast" and  
53 "slow" decays respectively to NPs aggregates' and dipolar chains motion. Indeed, Figure 3b  
54  
55  
56  
57  
58  
59  
60

indicates that dipolar chains start forming after  $\sim 30$  s, making their presence very likely at  $t = 2$  min. To take into account their bimodal character, we describe the normalized  $g_2 - 1$  data measured under magnetic field with the following two KWW relaxation modes:

$$\frac{g_2(\mathbf{q}, \tau) - 1}{B} = \left[ A(\mathbf{q}) \exp\left(\frac{\tau}{\tau_f(\mathbf{q})}\right)^{\beta_f(\mathbf{q})} + (1 - A(\mathbf{q})) \exp\left(\frac{\tau}{\tau_s(\mathbf{q})}\right)^{\beta_s(\mathbf{q})} \right]^2. \quad (4)$$

where  $\tau_f$  and  $\tau_s$  are the "fast" and "slow" modes characteristic decorrelation times,  $\beta_f$  and  $\beta_s$  are the corresponding KWW exponents, and  $A$  is the  $q$ -dependent amplitude of the corresponding decay. Our analysis of the collective dynamics under magnetic field focuses on the fast decorrelation time induced by the NPs aggregates resulting in an average relaxation time defined as  $\tau_c = \tau_f/\beta_f \Gamma(1/\beta_f)$ . Both  $\tau_c$  and  $\beta_f$  are shown in the inset of Figure 5. Similarly as in the previous section, we observe that the autocorrelation functions always decorrelate following a compressed exponential profile. However, the characteristic times  $\tau_c$  are strikingly twenty times shorter here. This accelerated collective dynamics is undoubtedly due to the magnetic field induced displacement of the NPs aggregates within the matrix and it represents another direct experimental evidence that NPs aggregates move to large distances when submitted to the magnetic stimulus. In addition, the exponent  $\beta_f$  is found to be almost constant and close to  $1.68 \pm 0.07$ , similar to the value obtained without magnetic field. In line with our above hypotheses, this result suggests therefore that the hyperdiffusive character is related to the nature of the sample, i.e., that apart from NPs polydispersity effects, the polymer-NPs interactions and the persisting structuration in the liquid TPU strongly impact the NPs dynamics.

Besides, Figure 5 inset shows that the power-law exponent of  $\tau_c(q)$  is  $-0.89 \pm 0.02$ , being significantly higher than the one found in absence of magnetic field and closer to -1, as in a typical ballistic-like stress relaxations mechanism. We interpret this result as a consequence of the magnetic interactions arising between NPs in presence of the magnetic field. In fact, although the magnetization of the NPs occurs along the vertical direction, the magnetic

1  
2  
3 dipolar interactions between NPs must also generate horizontal forces and corresponding  
4 NPs motion, eventually leading to the formation of large dipolar chains containing several  
5 NPs in their section as evidenced in Figure 2b. In other words, because the horizontal com-  
6 ponent of the NPs displacement is mainly driven by attractive dipolar interactions between  
7 NPs (and local excluded volume effects satisfying NPs non-interpenetration), a ballistic-like  
8 dynamic is not surprising here. When there are significant affine motions of particles and  
9 their clusters in the sample, three mechanisms contribute to the apparent value of the KWW  
10 exponent and the  $q$ -dependence of the relaxation time.<sup>30,36</sup> First, the transit of the particles  
11 across the beam determined by the mean velocity, which is  $q$ -independent. Second, the main  
12 advective contribution due to the velocity differences from the mean velocity, which can be  
13 linear or quadratic in inverse  $q$  according to the velocity distribution function. Finally, the  
14 diffusive term, which is quadratic in inverse  $q$ . As a result, the utilization of the KWW  
15 function can theoretically provide any exponent between 0 and -2 for the  $q$ -dependence of  
16 the relaxation time depending on the relative contributions of the three terms.<sup>37</sup>  
17  
18  
19  
20  
21  
22  
23  
24  
25  
26  
27  
28  
29  
30  
31  
32

33 In Figure 6, we show the normalized autocorrelation functions obtained at  $t = 19 \text{ min}$   
34 and  $T = 187 \pm 1 \text{ }^\circ\text{C}$ . Strikingly, we observe that the collective microscopic dynamic is much  
35 slower than at  $t = 2 \text{ min}$ . In fact, the characteristic times  $\tau_c$  reported here are found to  
36 be comparable, albeit slightly shorter, than those observed in absence of magnetic field that  
37 are, ca. 10 times longer than at  $t = 2 \text{ min}$ . To explain this slower collective dynamics,  
38 one can invoke stronger dipolar interactions between NPs in the dipolar chains, represent-  
39 ing the final stage of the structural evolution of the nanocomposite where NPs motion is  
40 significantly hindered albeit not fully suppressed. The corresponding values of  $\tau_c$  and  $\beta_f$   
41 obtained through fits based on Eq. 4 are reported in the inset. The collective microscopic  
42 dynamics appears to be hyperdiffusive, as indicated by the value of  $\beta = 1.87 \pm 0.17$ . In  
43 addition, the power-law exponent characterizing  $\tau_c(q)$  is here  $-1.30 \pm 0.01$ , indicating again  
44 a prevalent ballistic-like dynamical behavior, as expected in presence of the magnetic field  
45  
46  
47  
48  
49  
50  
51  
52  
53  
54  
55  
56  
57  
58  
59  
60

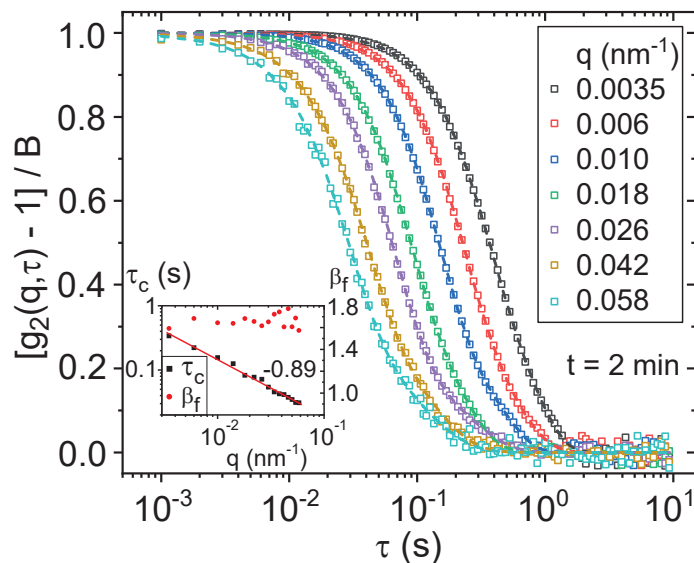


Figure 5: Normalized intensity-intensity autocorrelation functions at  $188 \pm 2 \text{ }^\circ\text{C}$  for different scattering vector moduli of the 5% Fe-n composite after 2 *min* from the activation of the magnetic field. Dashed lines are fit to the experimental data according to Eq. 4. Inset: average characteristic decorrelation time ( $\tau_c$ ) and KWW exponent ( $\beta_f$ ) obtained from the fit of the intensity-intensity autocorrelation functions shown in the main figure. The solid line is a power-law fit of  $\tau_c(q)$  providing an exponent of  $-0.89 \pm 0.02$ .

generating dipolar interaction between NPs. However, the difference between the  $\tau_c(q)$  exponents obtained at  $t = 2 \text{ min}$  and  $t = 19 \text{ min}$ , being respectively  $-0.89$  and  $-1.3$  is significant, which indicates that the advective contribution is relatively weaker at  $19 \text{ min}$  as compared to  $2 \text{ min}$  in agreement with the progressive formation of dipolar chains. A precise separation of the different contributions is however challenging because of the complexity of the material and the nature of the solicitation that we applied. Further investigations on model samples are therefore needed to clarify the influence of the different contributions to the collective microscopic dynamics.

For the sake of clarity, we show in Figure 7 the direct comparison of the characteristic times  $\tau_c$  obtained at different  $q$  in absence of the magnetic field as well as after 2 *min* and 19 *min* of induction heating. This figure illustrates the main discovery of our study and is probably relevant to develop future applications since it has been measured on an

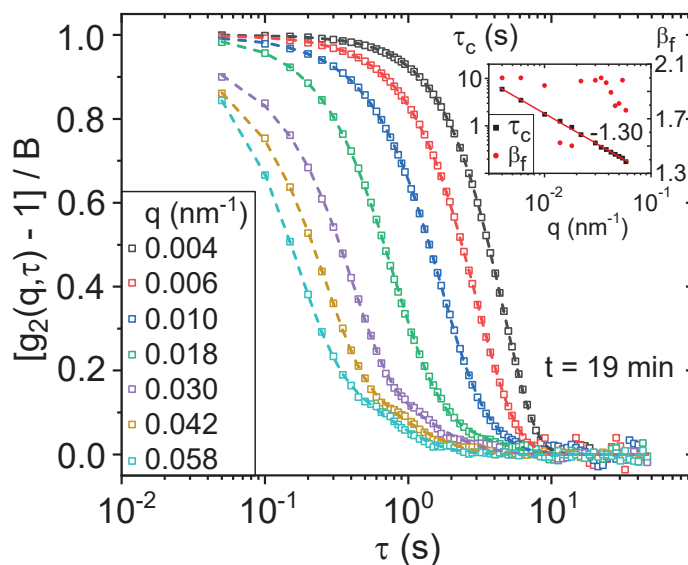


Figure 6: Normalized intensity-intensity autocorrelation functions at  $187 \pm 1$  °C for different scattering vector moduli of the 5% Fe-n composite at  $t = 19$  min. Dashed lines are fit to the experimental data according to Eq. 4. Inset: corresponding average decorrelation time ( $\tau_c$ ) and KWW exponent ( $\beta_f$ ) obtained from the fit. The solid line is a power-law fit of  $\tau_c(q)$  providing an exponent of  $-1.30 \pm 0.01$ .

industrially-oriented well-healable 5% Fe-n composite.<sup>8</sup> It clearly shows the non-monotonic behavior of the NP dynamics, first accelerated by the activation of the magnetic field and the subsequent polymer melting, before to be slowed down by the formation of massive dipolar chains within the material.

To go deeper into the physical understanding of the extra-heating process, which appears crucial to build a quantitative model capable of predicting the temperature evolution upon induction heating, we provide below some elements of discussion. One can notably wonder about the origin of the heat generated through friction. In particular, is friction mainly driven by the translational or rotational motion of NPs? Here, it is worth mentioning that XPCS measurements cannot directly answer this question. In fact, being XPCS not sensitive to the rotation of spherical particles (but only to their translation), it is here impossible to measure quantitatively the NPs tangential velocity, their deflection angle, nor the number of rotation events per second. However, a strong argument to reply to this question lies in our

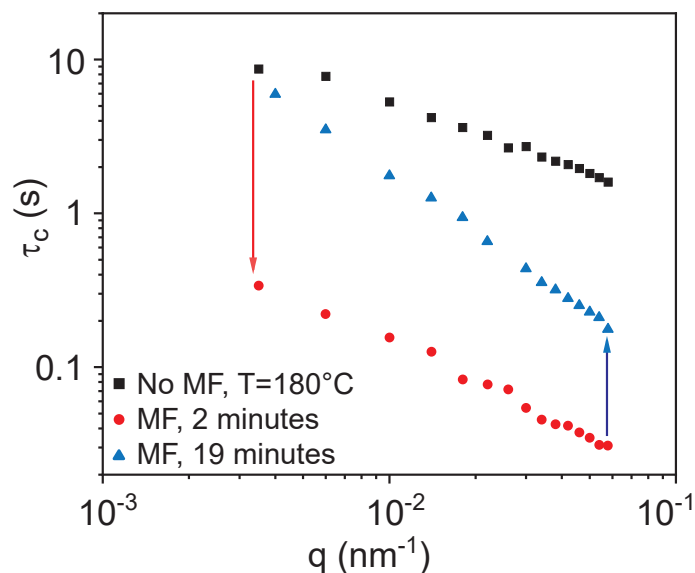


Figure 7: Comparison of the  $\tau_c$  values obtained at different scattering vector moduli in absence of magnetic field (black square data,  $T = 180\text{ }^\circ\text{C}$ ) as well as after 2 *min* (red circle data,  $T = 188\text{ }^\circ\text{C}$ ) and 19 *min* (blue triangle data,  $T = 187\text{ }^\circ\text{C}$ ) of induction heating. The red and blue arrows are guides for the eye to highlight the dynamical transitions. The red arrow emphasizes the acceleration of the dynamics when heating comes from the magnetic field instead of a hot-stage. The blue arrow emphasizes the NPs motion slowing down upon dipolar chain formation occurring at long time.

measurements of both static structure and dynamics after 19 *min* of magnetic irradiation. In this case, the static structure is known to be stable (Figure 3b) and the translational dynamics relatively slow (Figure 6-7), meaning that the cumulated displacement of NPs per time unit is rather low. However, looking at the temperature evolution in Figure 3a clearly shows that  $T_{\text{plateau}}$  ( $\approx 187\text{ }^\circ\text{C}$ ) is significantly higher than the prediction provided by Eq. 1 at long time ( $\approx 125\text{ }^\circ\text{C}$ ), indicating that a significant amount of heat is generated by friction despite the very limited translational motion we detect. In consequence, the most plausible scenario involves motion at very short length- and timescales such as oscillatory rotations<sup>38,39</sup> and vibrations of NPs caused by local variations of the magnetic field, both generating heat without implying any static structure modification. We refer the reader to the recent article of Helbig et al.<sup>19</sup> where a theory for frictional superparamagnetic NPs is proposed, notably pointing that friction loss is the dominant heating mechanism at low

1  
2  
3 magnetic field amplitude and high frequency.  
4

5 At shorter experimental time, the presence of a maximum in temperature together with  
6 a strong acceleration of the NPs dynamics makes it tempting to correlate directly these  
7 phenomena. Indeed, one could argue that faster translational dynamics detected by XPCS  
8 right after the TPU melting point ( $t = 2 \text{ min}$ , see Figures 5 and 7) are directly responsible  
9 for the temperature increase through enhanced "translational friction". However, by simply  
10 considering that the heat dissipated through friction by time unit is the product of the  
11 polymer-NP interfacial velocity by the dragging force, itself proportional to the interfacial  
12 velocity, one can easily compare the situation of translational and rotational motions to have  
13 an idea of their relative weight in the friction phenomenon. For translation, the ballistic-like  
14 dynamics can be used to evaluate the velocity difference of NPs from their mean velocity  
15  $v_{translation} = \frac{1}{q\tau_c}$ , providing values in the range of  $300 - 350 \text{ nm s}^{-1}$  that gives an idea of  
16 the order of magnitude of the NPs translational speed. For rotation, however, the tangential  
17 velocity ( $v_{rotation}$ ) is expected to be a function of the magnetic field frequency  $f$ ,<sup>18</sup> assuming  
18 that the macrospin Néel relaxation time of the NP aggregates is much longer than  $1/f$ .  
19 This results in  $v_{rotation} = \frac{d_{agg}}{2} 2\pi f$ , where  $d_{agg}$  is the average size of the aggregates, providing  
20 values in the range  $5.0 \times 10^8$  and  $1.8 \times 10^9 \text{ nm s}^{-1}$ , roughly 6-7 orders of magnitude higher  
21 than in the case of translational motion. This ratio must then be squared when dealing with  
22 dissipated energy, making in consequence the contribution of the translational motion to  
23 the elevation of temperature completely negligible. Even if our estimation of the velocities  
24 are rough, and if other parameters such as the local complex viscosity (drag coefficient) or  
25 the geometry of the aggregates and the amplitude of the deflection angle are expected to  
26 impact the heat dissipation, they cannot reasonably reverse the trend. Therefore, beyond the  
27 general concept of friction evoked in the articles mentioned in introduction, we can conclude  
28 that the extra-heating process observed at the TPU melting point originates mainly from  
29 NPs rotation under cyclic magnetic field. Determining precisely the contribution of each  
30 type of motion is however not an easy task in our material (where the matrix is biphasic  
31  
32  
33  
34  
35  
36  
37  
38  
39  
40  
41  
42  
43  
44  
45  
46  
47  
48  
49  
50  
51  
52  
53  
54  
55  
56  
57  
58  
59  
60

1  
2  
3 and interacts selectively with NPs) and will certainly deserve further investigations, notably  
4  
5 varying the nature of the host polymer.  
6

7       Lastly, we want to point out that although changing the shape and size of the particles  
8  
9 is expected to have a strong impact on the material's ability to heat, quantitative predic-  
10  
11 tions are far from being trivial since they should consider both magnetic and mechanical  
12  
13 aspects contemporaneously. The model of Helbig et al.,<sup>19</sup> dealing with the simplest case,  
14  
15 i.e., spherical superparamagnetic NPs suspended in a Newtonian liquid, already evidences  
16  
17 the complexity of the task. Incorporating the physics of multidomain magnetic NPs as well  
18  
19 as possible structural evolution with time in a non-Newtonian fluid (as it is the case in  
20  
21 the present work) appears therefore as a major challenge that will have to be addressed  
22  
23 progressively in the coming years.  
24  
25

## 26 27 **Conclusion**

28  
29 To summarize, we have used *in situ* time-resolved ultra small-angle X-ray scattering and X-  
30  
31 ray photon correlation spectroscopy to investigate the evolution of the static structure and  
32  
33 the collective microscopic dynamics of an industrially relevant responsive nanocomposite  
34  
35 during induction heating. By combining both experimental techniques with a follow-up of  
36  
37 the temperature through IR imaging, we have clarified the physical origin of the second  
38  
39 heating source appearing at the dissociation point (or melting) of soft systems containing  
40  
41 magnetic nanoparticles. The friction generated by the particles rotation is undoubtedly  
42  
43 responsible for this additionnal heating.  
44

45       Besides, we have highlighted the complex history of our healable nanocomposite from  
46  
47 the activation of the oscillatory magnetic field. The first stage involves Weiss domains walls  
48  
49 motion as the sole source of heat in the material, leading to an expected "Box-Lucas" expo-  
50  
51 nential rise of the temperature. Once the polymer melting region is reached, the temperature  
52  
53 is however seen to increase instead of saturate, owing to the triggering of a second heating-  
54  
55 process driven by particles rotation. Interestingly, after a few minutes, the temperature  
56  
57  
58  
59  
60

1  
2  
3 shows a maximum before stabilizing well above the prediction of the single exponential func-  
4 tion. This peculiar behavior indicates therefore that after its activation caused by the sudden  
5 drop of the viscosity at the polymer melting point, the friction process tends to become pro-  
6 gressively weaker, suggesting structural reorganization of the NPs. In fact, USAXS shows a  
7 rapid evolution of the static structure of the composite from the TPU melting point before  
8 to reach a stable configuration after a time corresponding to the observation of a maximum  
9 in temperature. Also, while XPCS reveals a strong acceleration of the NPs at the melting  
10 point, it unambiguously evidences their slowing down at longer times. These observations  
11 well agree with TEM micrographs revealing the presence of large dipolar chains at the end  
12 of the experiment, in which the heat produced by NPs friction is limited.

13  
14  
15 Finally, beyond fundamental understanding, our work illustrates the consequences of  
16 performing stimulus-healing of semi-crystalline polymers through induction heating. In par-  
17 ticular, it shows the complexity of the phenomena involved during the reparation of the  
18 material and reveals that long exposition to the magnetic field as well as multiple short  
19 healing steps ( $\approx 1 \text{ min}^8$ ) are very likely to modify significantly the structure of the NPs,  
20 altering both macroscopic properties and healing efficiency.

## 21 22 23 24 25 26 27 28 29 30 31 32 33 34 35 36 37 **Materials and Methods**

### 38 39 40 **Polymer matrix**

41  
42 The polymer matrix is a commercial TPU, (Desmopan 85085A, Covestro, Germany) with  
43  $M_w = 120 \text{ kg mol}^{-1}$  and molar-mass dispersity = 2. The full structure of the TPU chain is  
44 reported in ref. 8. The content in HDI-HDO-HDI hard segments is 28 wt.%. The soft seg-  
45 ments are made of two different motifs; SS1: butanediol polyadipate and SS2: polypropylene  
46 oxide (PPO) representing 50 wt.% and 22 wt.% of the polymer respectively.  
47  
48  
49  
50  
51  
52  
53  
54  
55  
56  
57  
58  
59  
60

## Magnetic Fillers

The magnetic fillers are iron nanoparticles (Fe-n NPs) (Nanografi, Turkey) with an original purity of 99.55 %. The range of particle sizes is 40 – 140 *nm*, with a mean particle size of ca. 100 *nm*.<sup>8</sup> A few micron particles are also observed. XRD diffractograms and FTIR spectra confirmed the particle's nature and purity and indicate the presence of an oxidized layer at the NPs surface.<sup>8</sup> The choice of these particles rely on their availability (cost) and ability to heat; the composite material presented in this work is produced at a pilot scale (5 kg) serving as a proof of concept for further development.

## Composites preparation

Appropriate amounts of TPU and NPs were used to prepare a composite filled with 5 *vol.%* in magnetic particles. They were hand-mixed at room temperature and then poured into a mini-extruder device (DSM Xplore, NL) equipped with two vertical co-rotative screws. The extruder chamber was pre-heated at 175 °C and the rotor speed was set to 80 *rpm*. After 5 *min* of extrusion, the nanocomposites were hot-pressed at 180 °C for 3 *min* under 100 *bars* and subsequently cooled down in air to room temperature in 10 *min*. The film thickness was fixed to 500  $\mu\text{m}$  in our experiments. The choice of the filler content (5 *vol.%*) was based on a previous series of physical characterization<sup>8</sup> that indicated a high enough heating ability while keeping a sufficient flowability in the molten state and satisfying mechanical properties in the solid state.

## Transmission Electron Microscopy (TEM)

Thin samples sections were prepared by cryo-ultramicrotomy at -80 °C and 0.3 *mm s*<sup>-1</sup> using an Ultracut UCT microtome (Leica, Germany) with a diamond knife (DiAtome, United Kingdom). Sections of approximately 90 *nm* thick were dry-collected and placed on a 400-mesh copper grid. TEM images were acquired using a CM120 transmission electron microscope, Philips, operating at an accelerating voltage of 120 *kV*.

## Focused Ion Beam - Scanning Electron Microscopy (FIB-SEM)

Sectioning and imaging of the nanocomposites were performed using a dual column focused ion beam (FIB)-scanning electron microscope (SEM) ZEISS NVision40. A  $\text{Ga}^{2+}$  ion beam accelerated at 30 kV was used. A two step milling procedure was employed on the bulk nanocomposites, which had been metallized with gold beforehand. First, a bulk trapezoid was milled at high current beam (4 nA) so that the shorter face could be imaged by the electron beam up to depth of at least 15  $\mu\text{m}$ . Then, polishing of the observed surface was carried out with a fine current beam (80 pA). The SEM images of the polished surface were then recorded with an accelerating voltage of 5 kV, using an in-lens secondary electron (SE) detector.

## Induction Heating and Thermal Imaging

Induction heating was performed with a “Power Cube” generator of alternating current and a master controller v3+ apparatus (CEIA, Italy) connected to a two-turn coil continuously cooled-down by an inner water flow. The frequency of the magnetic field was set to 855  $\text{kHz}$  and its maximum amplitude in the sample to ca. 8  $\text{mT}$ . The irradiation of the sample was achieved through regularly spaced pulses (a 16.4  $\text{ms}$  pulse was started every 24.5  $\text{ms}$  representing a total of 67% of the experimental time), which resulted in a heating rate of ca. 13.3  $^{\circ}\text{C s}^{-1}$  at  $t = 0 \text{ s}$ . This value was chosen to trigger the melting of the material after a short enough time (relevant for TPU healing) while preventing thermal degradation. Note that because the power was maintained constant during the experiment, the initial heating rate and the maximum temperature were related to each other.

The temperature variations were recorded with a PI 450 infrared camera (Optris, Germany) equipped with a 13° lens characterized with an optical resolution of  $382 \times 288$  pixels and a measurement rate of 27  $\text{Hz}$ . At this rate, continuous measurements of the temperature were possible only for 15  $\text{min}$  before filling the maximum space available on the camera to store infrared images. Temperatures reported in this work refer systematically to the

1  
2  
3 maximal temperature recorded by the device in the region of interest. Data were processed  
4  
5 with the software Optix PIX Connect in the 0 – 250 °C temperature range.  
6  
7

## 8 9 **Ultra Small-Angle X-ray Scattering**

10  
11 Ultra small-angle X-ray scattering (USAXS) were carried on the polymer matrix and the  
12  
13 nanocomposite loaded with 5 *vol.%* in Fe-n NPs at room temperature and under resistive  
14  
15 or induction heating, on the ID02 beamline at ESRF Grenoble, France. Details on the  
16  
17 experimental setup of the beamline and how data reduction was performed to obtain the  
18  
19 scattering intensity in absolute units ( $cm^{-1}$ ) can be found in ref. 40. We used different  
20  
21 sample to detector distances to cover a broad range of  $q$ . The experimental setup allowed  
22  
23 the investigation of a range of the modulus of  $q$ , i.e.,  $q = \frac{4\pi \sin \theta}{\lambda}$  with  $2\theta$  the scattering angle  
24  
25 and  $\lambda$  the X-ray wavelength, from  $2 \times 10^{-3} \text{ nm}^{-1}$  to  $2 \text{ nm}^{-1}$  (Figure 1). The contrast between  
26  
27 Fe NPs and the polymer matrix was very high and therefore the X-ray beam was attenuated  
28  
29 by a factor 33 to avoid detector saturation. Data acquisition was performed at a slow rate  
30  
31 with the fast beam shutter closed more than 90% of the time preventing any beam-induced  
32  
33 degradation effect.  
34

35  
36 During resistive heating, samples were placed in a Mettler heating stage which allowed a  
37  
38 controlled heating up to 180 °C. During induction heating, samples were placed within an  
39  
40 epoxy fiber composite strip, held using Kapton tape and suspended slightly above the center  
41  
42 of the coil to ensure X-ray transmission (see Figure 8). Time-resolved USAXS measurements  
43  
44 in the lowest- $q$  configuration were performed acquiring images every seconds from before the  
45  
46 activation of the induction heating and for the entire duration of the experiment (20 *min*).  
47  
48 The exposure time was approximately 100 *ms*. Most of the heat produced by the magnetic  
49  
50 field was dissipated in air by convection and a small part by conduction within the epoxy  
51  
52 strip.  
53  
54  
55  
56  
57  
58  
59  
60

## X-ray Photon Correlation Spectroscopy (XPCS)

X-ray Photon Correlation Spectroscopy (XPCS) measurements were carried on the 5% Fe-n composite in the same configuration used for USAXS measurements (see Figure 8). Speckle images were acquired as a function of the lag time  $\tau$  with a fixed time delay between two consecutive images that was varied accordingly to investigate the sample dynamics in the timescale range 1 *ms* to 100 *s*. The intensity variation of the acquired speckle pattern with time was analyzed in terms of the intensity-intensity autocorrelation function  $g_2$  measured as a function of the time delay  $\tau$  and scattering vector  $\mathbf{q}$ :

$$g_2(\mathbf{q}, \tau) = \frac{\langle I_p(\mathbf{q}, t) I_p(\mathbf{q}, t + \tau) \rangle_{t, \phi}}{\langle I_p(\mathbf{q}, t) \rangle_{t, \phi} \langle I_p(\mathbf{q}, t + \tau) \rangle_{t, \phi}} \quad (5)$$

with  $I_p(\mathbf{q}, t)$  the  $\mathbf{q}$  and time-dependent intensity measured by the  $p$ -th pixel, the brackets indicating the time average  $\langle \dots \rangle_t$  and the ensemble average  $\langle \dots \rangle_\phi$  over a ring of pixels centered around the transmitted beam position and characterized by the same magnitude of  $q$ .

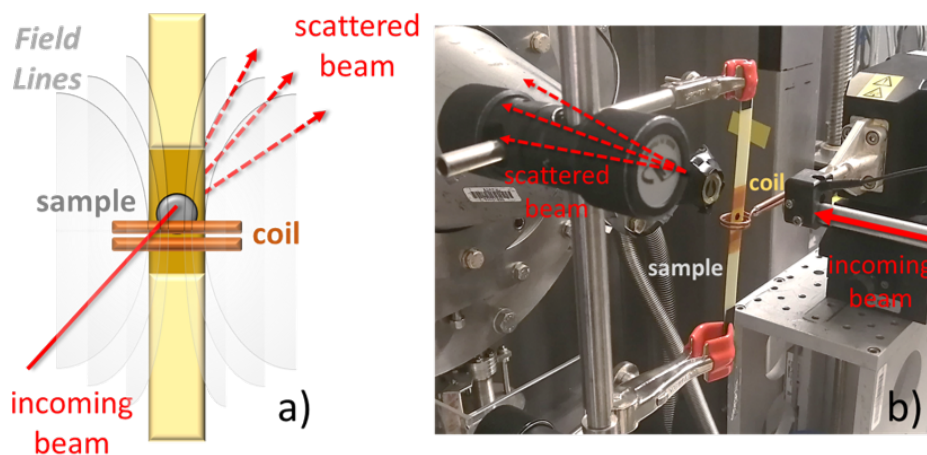


Figure 8: USAXS and XPCS experimental setup. a) Schematic front-view of the sample (gray circle) placed within the coil and the X-ray beam (red line) passing through the sample. Yellow and brown parts correspond to non-metallic materials. b) Photograph of the experimental setup at the ID02 beamline at ESRF.

## Magnetic properties characterization

The magnetisation measurements (Supporting Information section 1) of the powder and composites were performed using an ADE Magnetics EV7 Vibrating Sample Magnetometer at room temperature. The sample was placed inside a Teflon crucible and attached to a glass sample holder. A GMW electromagnet 3472-70 with maximum field strength of  $1.6 \times 10^6 \text{ Am}^{-1}$  and vibrating at a frequency of  $75 \text{ Hz}$  was used.

## Acknowledgement

P.G., G.C., F.M., J.B., S.M., and G.P.B. acknowledge the financial support of the Institut Carnot I@L for the funding assigned to the project POMMADE. G.P.B. acknowledges the financial of IDEX-Lyon and INSA-Lyon through the program ELAN-ERC. We acknowledge the European Synchrotron Radiation Facility for provision of synchrotron radiation facilities and the assistance in using beamline ID02. This publication has been partly developed thanks to the collaboration/networking within the SoftComp Consortium (<https://eu-softcomp.net>).

## Supporting Information Available

Magnetic properties characterization of the powder and the composite, additional details on the analysis of the affine dynamics and on the estimation of the size of the polymer nanodomains, the raw speckle images used to obtain the graphs presented in Figure 2a and 2b.

## References

1. Drobny, J. G. *Handbook of thermoplastic elastomers*; Elsevier, 2014.
2. Gaymans, R. J. Segmented copolymers with monodisperse crystallizable hard segments: Novel semi-crystalline materials. *Progress in polymer science* **2011**, *36*, 713–748.
3. Baeza, G. P. Recent advances on the structure–properties relationship of multiblock copolymers. *Journal of Polymer Science* **2021**, *59*, 2405–2433.
4. Cordier, P.; Tournilhac, F.; Soulié-Ziakovic, C.; Leibler, L. Self-healing and thermoreversible rubber from supramolecular assembly. *Nature* **2008**, *451*, 977–980.
5. Coey, J. M. *Magnetism and magnetic materials*; Cambridge university press, 2010.
6. Deatsch, A. E.; Evans, B. A. Heating efficiency in magnetic nanoparticle hyperthermia. *Journal of Magnetism and Magnetic Materials* **2014**, *354*, 163–172.
7. Bae, D.; Moon, M. J.; Shon, M. Y.; Oh, S. T.; Kim, G. N.; Yun, D. W. Study on the heating behavior of Ni-embedded thermoplastic polyurethane adhesive film via induction heating. *The Journal of Adhesion* **2017**, *93*, 964–979.
8. Griffiths, P.; Coativy, G.; Dalmas, F.; Falco, G.; Jiang, L.; Xiang, Z.; Le, M.-Q.; Ducharne, B.; Le Roy, D.; Méchin, F., *et al.* Ultrafast Remote Healing of Magneto-Responsive Thermoplastic Elastomer-Based Nanocomposites. *Macromolecules* **2022**, *55*, 831–843.
9. Corten, C. C.; Urban, M. W. Repairing polymers using oscillating magnetic field. *Advanced materials* **2009**, *21*, 5011–5015.
10. Ahmed, A. S.; Ramanujan, R. Magnetic field triggered multicycle damage sensing and self healing. *Scientific reports* **2015**, *5*, 1–10.

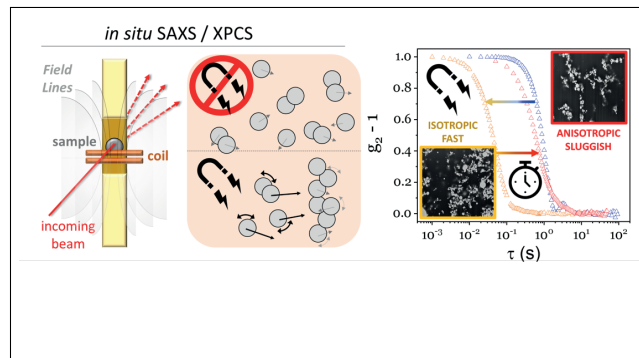
- 1  
2  
3 11. Panigrahi, R.; Zarek, M.; Sharma, V.; Cohn, D.; Ramanujan, R. V. Bio-Inspired Multiple  
4  
5 Cycle Healing and Damage Sensing in Elastomer–Magnet Nanocomposites. *Macromolec-*  
6  
7 *ular Chemistry and Physics* **2019**, *220*, 1900168.  
8  
9
- 10 12. Hohlbein, N.; Shaaban, A.; Schmidt, A. Remote-controlled activation of self-healing  
11  
12 behavior in magneto-responsive ionomeric composites. *Polymer* **2015**, *69*, 301–309.  
13  
14
- 15 13. Yang, Y.; He, J.; Li, Q.; Gao, L.; Hu, J.; Zeng, R.; Qin, J.; Wang, S. X.; Wang, Q. Self-  
16  
17 healing of electrical damage in polymers using superparamagnetic nanoparticles. *Nature*  
18  
19 *nanotechnology* **2019**, *14*, 151–155.  
20  
21
- 22 14. Baeza, G.; Griffiths, P.; Meille, S.; Coativy, G.; Mechin, F.; Bernard, J.; Robbiani, B.  
23  
24 Procédé de correction d'un défaut d'un matériau composite sous application d'un champ  
25  
26 magnétique (French patent FR2101537). 2022.  
27
- 28 15. Jiang, L.; Griffiths, P.; Balouet, J.; Faure, T.; Lyons, R.; Fustin, C.-A.; Baeza, G. P.  
29  
30 Magneto-Responsive Nanocomposites with a Metal–Ligand Supramolecular Matrix.  
31  
32 *Macromolecules* **2022**,  
33  
34
- 35 16. Hiergeist, R.; Andrä, W.; Buske, N.; Hergt, R.; Hilger, I.; Richter, U.; Kaiser, W. Ap-  
36  
37 plication of magnetite ferrofluids for hyperthermia. *Journal of magnetism and Magnetic*  
38  
39 *Materials* **1999**, *201*, 420–422.  
40  
41
- 42 17. Bayerl, T.; Schledjewski, R.; Mitschang, P. Induction heating of thermoplastic materials  
43  
44 by particulate heating promoters. *Polymers and Polymer Composites* **2012**, *20*, 333–342.  
45  
46
- 47 18. Yassine, O.; Zaher, A.; Li, E. Q.; Alfadhel, A.; Perez, J. E.; Kavaldzhiev, M.; Contr-  
48  
49 eras, M. F.; Thoroddsen, S. T.; Khashab, N. M.; Kosel, J. Highly efficient thermore-  
50  
51 sponsive nanocomposite for controlled release applications. *Scientific reports* **2016**, *6*,  
52  
53 1–7.  
54  
55  
56  
57  
58  
59  
60

- 1  
2  
3  
4  
5  
6  
7  
8  
9  
10  
11  
12  
13  
14  
15  
16  
17  
18  
19  
20  
21  
22  
23  
24  
25  
26  
27  
28  
29  
30  
31  
32  
33  
34  
35  
36  
37  
38  
39  
40  
41  
42  
43  
44  
45  
46  
47  
48  
49  
50  
51  
52  
53  
54  
55  
56  
57  
58  
59  
60
19. Helbig, S.; Abert, C.; Sánchez, P. A.; Kantorovich, S. S.; Suess, D. Self-consistent solution of magnetic and friction energy losses of a magnetic nanoparticle. *Physical Review B* **2023**, *107*, 054416.
  20. Baeza, G. P.; Sharma, A.; Louhichi, A.; Imperiali, L.; Appel, W. P.; Fitié, C. F.; Lettinga, M. P.; Ruymbeke, E. V.; Vlassopoulos, D. Multiscale Organization of Thermoplastic Elastomers with Varying Content of Hard Segments. *Polymer* **2016**, *107*, 89–101.
  21. Krajewski, M.; Lin, W. S.; Lin, H. M.; Brzozka, K.; Lewinska, S.; Nedelko, N.; Slawska-Waniewska, A.; Borysiuk, J.; Wasik, D. Structural and magnetic properties of iron nanowires and iron nanoparticles fabricated through a reduction reaction. *Beilstein journal of nanotechnology* **2015**, *6*, 1652–1660.
  22. Beaucage, G.; Kammler, H. K.; Pratsinis, S. E. Particle size distributions from small-angle scattering using global scattering functions. *Journal of applied crystallography* **2004**, *37*, 523–535.
  23. Baeza, G. P.; Genix, A.-C.; Degrandcourt, C.; Petitjean, L.; Gummel, J.; Couty, M.; Oberdisse, J. Multiscale filler structure in simplified industrial nanocomposite silica/SBR systems studied by SAXS and TEM. *Macromolecules* **2013**, *46*, 317–329.
  24. Yang, W.; Macosko, C.; Wellinghoff, S. Thermal degradation of urethanes based on 4,4'-diphenylmethane diisocyanate and 1,4-butanediol (MDI/BDO). *Polymer* **1986**, *27*, 1235–1240.
  25. Wildeboer, R.; Southern, P.; Pankhurst, Q. On the reliable measurement of specific absorption rates and intrinsic loss parameters in magnetic hyperthermia materials. *Journal of Physics D: Applied Physics* **2014**, *47*, 495003.
  26. Andreu, I.; Natividad, E. Accuracy of available methods for quantifying the heat power generation of nanoparticles for magnetic hyperthermia. *International Journal of Hyperthermia* **2013**, *29*, 739–751.

- 1  
2  
3 27. Zinn, T.; Sharpnack, L.; Narayanan, T. Phoretic dynamics of colloids in a phase sepa-  
4 rating critical liquid mixture. *Physical Review Research* **2020**, *2*, 033177.  
5  
6  
7  
8 28. Ramos, L.; Cipelletti, L. Ultraslow Dynamics and Stress Relaxation in the Aging of a  
9 Soft Glassy System. *Phys. Rev. Lett.* **2001**, *87*, 245503.  
10  
11  
12  
13 29. Bouchaud, J.-P.; Pitard, E. Anomalous dynamical light scattering in soft glassy gels.  
14 *Eur. Phys. J. E* **2001**, *6*, 231.  
15  
16  
17  
18 30. Bandyopadhyay, R.; Liang, D.; Yardimci, H.; Sessoms, D. A.; Borthwick, M. A.;  
19 Mochrie, S. G. J.; Harden, J. L.; Leheny, R. L. Evolution of Particle-Scale Dynamics in  
20 an Aging Clay Suspension. *Phys. Rev. Lett.* **2004**, *93*, 228302.  
21  
22  
23  
24 31. Falus, P.; Borthwick, M. A.; Narayanan, S.; Sandy, A. R.; Mochrie, S. G. J. Crossover  
25 from Stretched to Compressed Exponential Relaxations in a Polymer-Based Sponge  
26 Phase. *Phys. Rev. Lett.* **2006**, *97*, 066102.  
27  
28  
29  
30  
31 32. Srivastava, S.; Agarwal, P.; Mangal, R.; Koch, D. L.; Narayanan, S.; Archer, L. A.  
32 Hyperdiffusive Dynamics in Newtonian Nanoparticle Fluids. *ACS Macro Lett.* **2015**, *4*,  
33 1149.  
34  
35  
36  
37  
38 33. Schlotter, W. F.; Cionca, C.; Paruchuri, S. S.; Cunningham, J. B.; Dufresne, E.;  
39 Dierker, S. B.; Arms, D.; Clarke, R.; Ginder, J. M.; Nichols, M. E. The dynamics of  
40 magnetorheological elastomers studied by synchrotron radiation speckle analysis. *Inter-*  
41 *national Journal of Modern Physics B* **2002**, *16*, 2426–2432.  
42  
43  
44  
45  
46  
47 34. Nébouy, M.; de Almeida, A.; Chazeau, L.; Baeza, G. P. Modeling shear-induced crystal-  
48 lization in startup flow: The case of segmented copolymers. *Journal of Rheology* **2019**,  
49 *63*, 837–850.  
50  
51  
52  
53  
54 35. Morozov, I. A. Nanoindentation of polyurethane with phase-separated fibrillar structure.  
55 *Polym. Test.* **2021**, *94*, 107038.  
56  
57  
58  
59  
60

- 1  
2  
3  
4  
5  
6  
7  
8  
9  
10  
11  
12  
13  
14  
15  
16  
17  
18  
19  
20  
21  
22  
23  
24  
25  
26  
27  
28  
29  
30  
31  
32  
33  
34  
35  
36  
37  
38  
39  
40  
41  
42  
43  
44  
45  
46  
47  
48  
49  
50  
51  
52  
53  
54  
55  
56  
57  
58  
59  
60
36. Zinn, T.; Sharpnack, L.; Narayanan, T. Dynamics of magnetic Janus colloids studied by ultra small-angle X-ray photon correlation spectroscopy. *Soft Matter* **2023**, *19*, 2311–2318.
  37. Zinn, T.; Narayanan, T.; Kottapalli, S. N.; Sachs, J.; Sottmann, T.; Fischer, P. Emergent dynamics of light-induced active colloids probed by XPCS. *New Journal of Physics* **2022**, *24*, 093007.
  38. Usov, N.; Liubimov, B. Y. Dynamics of magnetic nanoparticle in a viscous liquid: Application to magnetic nanoparticle hyperthermia. *Journal of Applied Physics* **2012**, *112*, 023901.
  39. Suwa, M.; Uotani, A.; Tsukahara, S. Alignment and small oscillation of superparamagnetic iron oxide nanoparticle in liquid under alternating magnetic field. *Journal of Applied Physics* **2019**, *125*, 123901.
  40. Narayanan, T.; Sztucki, M.; Zinn, T.; Kieffer, J.; Homs-Puron, A.; Gorini, J.; Van Vaerenbergh, P.; Boesecke, P. Performance of the time-resolved ultra-small-angle X-ray scattering beamline with the Extremely Brilliant Source. *J. Appl. Crystallogr.* **2022**, *55*, 98–111.

## TOC Graphic



*in situ* SAXS / XPCS

